Intermediate vibronic coupling in charge transfer states

Stradomska, Anna; Kulig, Waldemar; Slawik, Michal; Petelenz, Piotr

Published in:
Journal of Chemical Physics

DOI:
10.1063/1.3597607

Publication date:
2011

Intermediate vibronic coupling in charge transfer states: Comprehensive calculation of electronic excitations in sexithiophene crystal

Anna Stradomska, Waldemar Kulig, Michał Slawik, and Piotr Petelenz

Citation: The Journal of Chemical Physics **134**, 224505 (2011); doi: 10.1063/1.3597607
View online: https://doi.org/10.1063/1.3597607
View Table of Contents: http://aip.scitation.org/toc/jcp/134/22
Published by the American Institute of Physics

Intermediate vibronic coupling in charge transfer states: Comprehensive calculation of electronic excitations in sexithiophene crystal

Anna Stradomska,[1,a)] Waldemar Kulig,[2] Michał Slawik,[2] and Piotr Petelenz[2]
[1]*Zernike Institute for Advanced Materials, University of Groningen, Nijenborgh 4, 9747 AG Groningen, The Netherlands*
[2]*K. Gumiński Department of Theoretical Chemistry, Jagiellonian University, Ingardena 3, 30-060 Kraków, Poland*

(Received 31 March 2011; accepted 16 May 2011; published online 13 June 2011)

A comprehensive theory of linear vibronic coupling in a coupled manifold of Frenkel and charge-transfer states in an infinite molecular crystal is presented and applied for sexithiophene. The approach, valid in the intermediate-coupling regime, includes up to three-particle terms of the Philpott expansion, with the vibronic wavefunctions represented in the Lang-Firsov basis. As a stringent test, the scheme is used to reproduce the complete set of available sexithiophene absorption and electroabsorption spectra within a unified theoretical framework. The input is based primarily on independent calculations and to some extent on independent experiments, with explicit fitting contained within the limits set by the estimated inherent errors of *a priori* parameter estimates. Reasonably good quantitative agreement with experimental spectra is achieved. The results resolve some existing interpretational ambiguities and expose some peculiarities of electric field effect on vibronic eigenstates of Frenkel parentage, highlighting the role of charge-transfer interactions. © *2011 American Institute of Physics*. [doi:10.1063/1.3597607]

I. INTRODUCTION

Operation of optoelectronic devices, such as OLEDs, is rooted in mutual transformations between different kinds of electronic excitation, namely, between free charge carriers, which mediate the strong coupling of the active components to external electric field and charge reservoir, and Frenkel excitons, which couple the system to light waves. In Frenkel (intramolecular) excitons, the excited electron and the hole created in the ground-state Fermi sea are located at the same molecule, while in an unbound electron-hole pair the two charge carriers are separated by a distance large enough to make their interaction negligible. The excitations existing in the intermediate region of finite electron-hole distances are usually referred to as charge-transfer (CT) excitons. Acting as precursors in charge carrier photogeneration[1] and as intermediates in charge carrier recombination,[2] they play a pivotal role and deserve to be very thoroughly studied.

These studies are obstructed by the low absorption intensity of charge transfer states. In fact, in order to create such an exciton, an electron must be transferred from one molecule to another, so that the corresponding transition dipole is limited by the (small) intermolecular overlap integral. In addition to this inherent transition dipole moment, the CT states borrow some from the Frenkel states,[3] to which they are coupled by charge transfer integrals (in this context called exciton-dissociation integrals). However, the latter are also limited by intermolecular overlap, and hence are rather small; moreover, the corresponding bands are usually masked by intense vibrational satellites of Frenkel states. Consequently, apart from some exceptional cases of crystals with rather special structure, observed in specific orientations,[4] the absorption intensity of CT excitons is usually marginal when compared to intramolecular excitations which dominate the absorption spectra.

In effect, CT excitons can be experimentally probed almost exclusively by electro-absorption (EA) spectroscopy[5–7] which consists in measuring the response of the absorption spectrum to modulation by external electric field. The large field-induced shifts of the CT states (due to their large dipole moments) compensate their low absorption intensity, ultimately producing signals comparable in amplitude and reasonably well discernible from those of Frenkel excitons. Unfortunately, EA spectroscopy is not a commonly used technique, so that the set of available data is limited. Until new results become accessible, this emphasizes the need to explore to the utmost existing experimental spectra.

In this regard, the sexithiophene (6T) case presents itself as an unprecedented opportunity. On the one hand, the system is interesting in a broader context as a representative of the oligothiophene family, already applied in field-effect transistors and light-emitting diodes;[8–11] this adds impact to the potential conclusions concerning its excited states, especially of CT parentage. On the other hand, it is one of the very few organic single crystals for which the EA spectrum has been published,[12] offering considerable interpretational advantage with respect to the more common spectra of organic films.[4,8] Last but not least, it is one of the rare cases where the CT states are clearly observable also in absorption spectroscopy.[4]

This last circumstance suggests an attempt to reproduce the absorption and electroabsorption spectrum of 6T within the same internally consistent model as a new and stringent

a)Electronic mail: a.u.stradomska@rug.nl.

test of the existing theoretical understanding in this field. So far, theoretical description of the EA spectra[13] was focused on CT states, with only scant attention given to Frenkel excitons and to vibronic coupling, crucial just for these latter states, but less relevant for CT excitations. This obstructed meaningful application for absorption spectra, making it practically impossible for *ac* polarization where intramolecular excitations prevail. In contrast, the existing detailed interpretations of absorption spectra[14–19] completely ignored the existence of the CT manifold, precluding interpretation of EA spectra, but also of *b*-polarized absorption, where (owing to specific lattice structure) the CT contribution is prominent.

In this paper, we present a theoretical model where vibronic effects are consistently handled in the space spanned both by the Frenkel and CT electronic excitations, which enables us to treat the absorption and electroabsorption spectra on equal footing, referring to the complete experimental material available to date. The approach is valid in the sensitive region of intermediate vibronic coupling, providing a comprehensive framework in which to treat the same problem in a variety of molecular crystals.

II. MODEL HAMILTONIAN

The model crystal is represented as a rigid, infinite, three-dimensional lattice with M molecules per unit cell. A molecule is identified by a pair of descriptors: the vector $\boldsymbol{n}$ of crystallographic indices determines the unit cell in which the molecule is located, while the sublattice index $\alpha = 1, 2, \ldots, M$ specifies both the position and orientation of the molecule within the unit cell.

Excited states of such a crystal are constructed as linear combinations of localized excitations. The electronic excited states that we take into account include one dipole-allowed, intramolecular (Frenkel) state per molecule and a set of charge-transfer states with electron-hole distances limited to a small range, carefully chosen for the crystal in hand. Specifically, for the sexithiophene crystal we consider the CT states with electron and hole located on the nearest and second-nearest neighbours within the same dense-packing plane (see Fig. 1). In our model, these states and the Frenkel state are coupled to one (effective) intramolecular vibrational mode per molecule. We assume the vibrational potential to be harmonic and of the same curvature in all the electronic states considered: in the ground electronic state, excited state, as well as in the cationic and anionic forms of the molecule. The only change it undergoes upon excitation or ionization is linear in the vibrational coordinate, resulting in the shift of the potential minimum along the (dimensionless) vibrational coordinate by the corresponding Franck-Condon parameter. In general, this shift may be different for the excited state, for the cation, and for the anion.

In the following, $A^\dagger_{\boldsymbol{n}\alpha}$ denotes the operator that creates the Frenkel state on the molecule $\boldsymbol{n}\alpha$, $X^\dagger_{\boldsymbol{n}\alpha,\boldsymbol{m}\beta}$ creates the CT state with the hole on the molecule $\boldsymbol{n}\alpha$ and the electron on the molecule $\boldsymbol{m}\beta$, while $b^\dagger_{\boldsymbol{n}\alpha}$ creates one vibrational quantum on the molecule $\boldsymbol{n}\alpha$ in the potential of the electronic ground state of the neutral molecule. This notation seems optimal

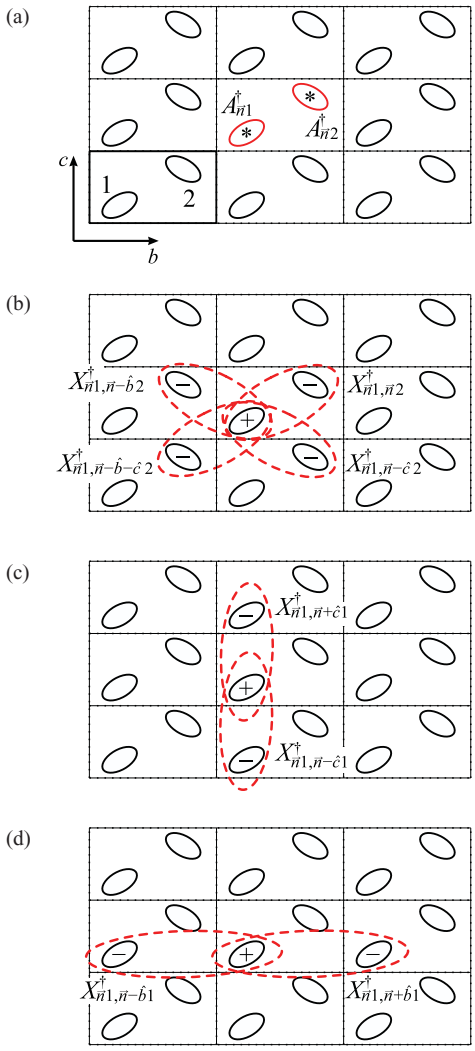

FIG. 1. Examples of localized states used for sexithiophene crystal. A 3 × 3 unit cells fragment of the dense-packing *bc* crystal plane is shown. Crystallographic coordinates of the central unit cell are given by $\boldsymbol{n}$. The orientation of axes *b* and *c* as well as the numbering of the molecules within the unit cell are indicated in the left bottom corner of Fig. (a). (a) Frenkel states, (b) charge-transfer states with the hole in the unit cell $\boldsymbol{n}$ and the electron located on the nearest neighbour of the hole, (c) charge-transfer states with the hole in unit cell $\boldsymbol{n}$ and electron located on the second neighbour along the shortest basic translation *c*, (d) charge-transfer states with the hole in unit cell $\boldsymbol{n}$ and electron located on the second neighbour along the basic translation *b*. Only the charge-transfer states with the hole on sublattice 1 are shown, the corresponding states with the hole on sublattice 2 are obtained by trivial interchange.

for our present focus on vibronic coupling. However, a different one was used in the previous papers dealing specifically with the Frenkel-CT state mixing.[13,20] As reference to those papers may be relevant to a reader interested in some details, Appendix B shows the correspondence between the two conventions.

The Hamiltonian for the model crystal, correct to terms linear in intermolecular overlap integrals between neighbouring molecules and in the Heitler-London approximation, reads

$$H = H_F + H_{CT} + H_{ph} + H_{F-CT} + H_{F-ph} + H_{CT-ph}, \tag{1}$$

$$H_F = \sum_{\boldsymbol{n},\alpha} E^F(\boldsymbol{F}) A^\dagger_{\boldsymbol{n}\alpha} A_{\boldsymbol{n}\alpha} + \sum_{\substack{\boldsymbol{n},\alpha \\ \boldsymbol{m},\beta}}{}' J_{\alpha\beta}(\boldsymbol{r}_{\boldsymbol{m}\beta} - \boldsymbol{r}_{\boldsymbol{n}\alpha}) A^\dagger_{\boldsymbol{n}\alpha} A_{\boldsymbol{m}\beta}, \tag{2}$$

$$\begin{aligned} H_{CT} = &\sum_{\substack{\boldsymbol{n},\alpha \\ \boldsymbol{l},\gamma}}{}'' E^{CT}_{\alpha\gamma \boldsymbol{l}-\boldsymbol{n}}(\boldsymbol{F}) X^\dagger_{\boldsymbol{n}\alpha,\boldsymbol{l}\gamma} X_{\boldsymbol{n}\alpha,\boldsymbol{l}\gamma} \\ &+ \sum_{\substack{\boldsymbol{n},\alpha \\ \boldsymbol{m},\beta}}{}' \sum_{\boldsymbol{l},\gamma}{}'' T^e_{\alpha\beta}(\boldsymbol{r}_{\boldsymbol{m}\beta} - \boldsymbol{r}_{\boldsymbol{n}\alpha}) X^\dagger_{\boldsymbol{l}\gamma,\boldsymbol{n}\alpha} X_{\boldsymbol{l}\gamma,\boldsymbol{m}\beta} \\ &+ \sum_{\substack{\boldsymbol{n},\alpha \\ \boldsymbol{m},\beta}}{}' \sum_{\boldsymbol{l},\gamma}{}'' T^h_{\alpha\beta}(\boldsymbol{r}_{\boldsymbol{m}\beta} - \boldsymbol{r}_{\boldsymbol{n}\alpha}) X^\dagger_{\boldsymbol{n}\alpha,\boldsymbol{l}\gamma} X_{\boldsymbol{m}\beta,\boldsymbol{l}\gamma}, \end{aligned} \tag{3}$$

$$H_{ph} = \sum_{\boldsymbol{n},\alpha} \hbar\omega b^\dagger_{\boldsymbol{n}\alpha} b_{\boldsymbol{n}\alpha}, \tag{4}$$

$$\begin{aligned} H_{F-CT} = &\sum_{\substack{\boldsymbol{n},\alpha \\ \boldsymbol{l},\gamma}}{}'' D^e_{\gamma\alpha}(\boldsymbol{r}_{\boldsymbol{n}\alpha} - \boldsymbol{r}_{\boldsymbol{l}\gamma}) X^\dagger_{\boldsymbol{n}\alpha,\boldsymbol{l}\gamma} A_{\boldsymbol{n}\alpha} + h.c. \\ &+ \sum_{\boldsymbol{n},\alpha} \sum_{\boldsymbol{l},\gamma}{}'' D^h_{\alpha\gamma}(\boldsymbol{r}_{\boldsymbol{l}\gamma} - \boldsymbol{r}_{\boldsymbol{n}\alpha}) X^\dagger_{\boldsymbol{n}\alpha,\boldsymbol{l}\gamma} A_{\boldsymbol{l}\gamma} + h.c., \end{aligned} \tag{5}$$

$$H_{F-ph} = \sum_{\boldsymbol{n},\alpha} \hbar\omega\lambda_F A^\dagger_{\boldsymbol{n}\alpha} A_{\boldsymbol{n}\alpha} (b^\dagger_{\boldsymbol{n}\alpha} + b_{\boldsymbol{n}\alpha}), \tag{6}$$

$$H_{CT-ph} = \sum_{\substack{\boldsymbol{n},\alpha \\ \boldsymbol{l},\gamma}}{}'' \hbar\omega X^\dagger_{\boldsymbol{n}\alpha,\boldsymbol{l}\gamma} X_{\boldsymbol{n}\alpha,\boldsymbol{l}\gamma} [\lambda_h (b^\dagger_{\boldsymbol{n}\alpha} + b_{\boldsymbol{n}\alpha}) + \lambda_e (b^\dagger_{\boldsymbol{l}\gamma} + b_{\boldsymbol{l}\gamma})]. \tag{7}$$

Single prime in Eqs. (2)–(7) means that the term with $\boldsymbol{n}\alpha = \boldsymbol{m}\beta$ is omitted in the summation, while double prime indicates the omission of all terms with $\boldsymbol{l}\gamma$ that would lead to the appearance of the creation/anihiliation operators for CT states with the electron-hole distance from outside of the chosen set. Here, $E^F(\boldsymbol{F})$ and $E^{CT}_{\alpha\beta\boldsymbol{m}}(\boldsymbol{F})$ stand for the vertical excitation energies of the localized Frenkel state and of a charge-transfer state with the hole on sublattice α and the electron on sublattice β, $\boldsymbol{m}$ unit cells from the hole. The effect of external electric field ($\boldsymbol{F}$) on these energies is explicitly included as

$$E^i(\boldsymbol{F}) = E^i(\boldsymbol{0}) - \boldsymbol{m}_i \cdot \boldsymbol{F} - \frac{1}{2} p_i \boldsymbol{F}^2, \tag{8}$$

where $\boldsymbol{m}_i$ and p_i denote the permanent dipole moment and polarizability change upon the creation of the localized excited state i (Frenkel or CT). Based on the fundamental reference[21] and following our previous paper[13] on 6T spectroscopy, the electric field strength is taken as the geometric mean of the macroscopic and local electric field, the latter being approximated by the isotropic Lorentz formula.

The interaction between Frenkel states located on molecules at a relative distance $\boldsymbol{r}$ on sublattice α and β, respectively, is mediated by the resonance interaction integral $J_{\alpha\beta}(\boldsymbol{r})$. The coupling between Frenkel and CT states is governed by electron and hole dissociation integrals $D^e_{\alpha\beta}(\boldsymbol{r})$ and $D^h_{\alpha\beta}(\boldsymbol{r})$, while the coupling within the subspace of CT states is mediated by electron and hole transfer integrals $T^e_{\alpha\beta}(\boldsymbol{r})$ and $T^h_{\alpha\beta}(\boldsymbol{r})$.

The vibrational quantum energy is $\hbar\omega$. The Huang-Rhys factors λ_F^2, λ_h^2, and λ_e^2 for the molecular excited state, cation, and anion, respectively, correspond to dimensionless Franck-Condon displacement parameters of $\sqrt{2}\lambda_F$, $\sqrt{2}\lambda_h$, and $\sqrt{2}\lambda_e$.

In order to diagonalize the model Hamiltonian, we use the displaced-oscillator basis set[22] and the three-particle approximation.[23] One-, two- and three-particle localized Frenkel states

$$|\boldsymbol{n}_1\alpha_1 \overset{*}{v}_1\rangle = \frac{A^\dagger_{\boldsymbol{n}_1\alpha_1} (\overset{*}{b}{}^\dagger_{\boldsymbol{n}_1\alpha_1})^{v_1}}{\sqrt{v_1!}} |0\rangle, \tag{9}$$

$$|\boldsymbol{n}_1\alpha_1 \overset{*}{v}_1 (\boldsymbol{n}_2\alpha_2 v_2)\rangle = \frac{A^\dagger_{\boldsymbol{n}_1\alpha_1} (\overset{*}{b}{}^\dagger_{\boldsymbol{n}_1\alpha_1})^{v_1} (b^\dagger_{\boldsymbol{n}_2\alpha_2})^{v_2}}{\sqrt{v_1! v_2!}} |0\rangle, \tag{10}$$

$$\begin{aligned} &|\boldsymbol{n}_1\alpha_1 \overset{*}{v}_1 (\boldsymbol{n}_2\alpha_2 v_2, \boldsymbol{n}_3\alpha_3 v_3)\rangle \\ &= \frac{A^\dagger_{\boldsymbol{n}_1\alpha_1} (\overset{*}{b}{}^\dagger_{\boldsymbol{n}_1\alpha_1})^{v_1} (b^\dagger_{\boldsymbol{n}_2\alpha_2})^{v_2} (b^\dagger_{\boldsymbol{n}_3\alpha_3})^{v_3}}{\sqrt{v_1! v_2! v_3!}} |0\rangle, \end{aligned} \tag{11}$$

correspond to the state with one, two, or three molecules in the crystal being excited: one of them ($\boldsymbol{n}_1\alpha_1$) is excited both electronically and vibrationally, and the remaining molecules (one in the case of a two-particle state, or two in the case of a three-particle state) are excited vibrationally (see Fig. 2). We use the operator with the asterisk $\overset{*}{b}{}^\dagger_{\boldsymbol{n}\alpha}$ to indicate that the vibrational quanta are created in the "displaced" potential of the electronic excited state, in contrast to "standard" creation operator $b^\dagger_{\boldsymbol{n}\alpha}$ which creates phonons in the "undisplaced" potential of the electronic ground state. Similarly, $\overset{*}{v}$ is used to denote the number v of phonons in the displaced potential of the electronic excited state.

The two- and three-particle localized charge-transfer states

$$|\boldsymbol{n}_1\alpha_1 \overset{+}{v}_1, \boldsymbol{n}_2\alpha_2 \overset{-}{v}_2\rangle = \frac{X^\dagger_{\boldsymbol{n}_1\alpha_1,\boldsymbol{n}_2\alpha_2} (\overset{+}{b}{}^\dagger_{\boldsymbol{n}_1\alpha_1})^{v_1} (\overset{-}{b}{}^\dagger_{\boldsymbol{n}_2\alpha_2})^{v_2}}{\sqrt{v_1! v_2!}} |0\rangle, \tag{12}$$

$$\begin{aligned} &|\boldsymbol{n}_1\alpha_1 \overset{+}{v}_1, \boldsymbol{n}_2\alpha_2 \overset{-}{v}_2 (\boldsymbol{n}_3\alpha_3 v_3)\rangle \\ &= \frac{X^\dagger_{\boldsymbol{n}_1\alpha_1,\boldsymbol{n}_2\alpha_2} (\overset{+}{b}{}^\dagger_{\boldsymbol{n}_1\alpha_1})^{v_1} (\overset{-}{b}{}^\dagger_{\boldsymbol{n}_2\alpha_2})^{v_2} (b^\dagger_{\boldsymbol{m}\beta})^{w}}{\sqrt{v_1! v_2! v_3!}} |0\rangle, \end{aligned} \tag{13}$$

describe the state of the crystal with two molecules ionized and excited vibrationally ($\boldsymbol{n}_1\alpha_1$ carrying a hole and $\boldsymbol{n}_2\alpha_2$ carrying an electron) and, in the case of a three-particle state, one extra molecule excited purely vibrationally (see Fig. 3). In complete analogy to the case of Frenkel states, we use $\overset{+}{b}{}^\dagger_{\boldsymbol{n}\alpha}$ and $\overset{-}{b}{}^\dagger_{\boldsymbol{n}\alpha}$ to denote the creation operators for phonons in the displaced potential of the cation and of the anion, while $\overset{+}{v}$ and $\overset{-}{v}$ denote the number v of phonons in the displaced potentials of the corresponding ionized states.

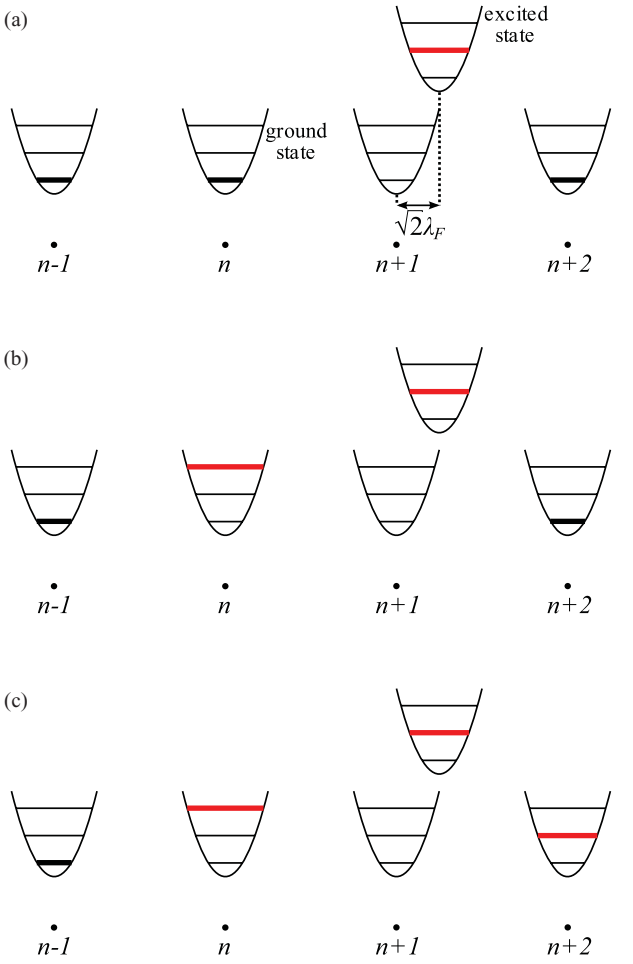

FIG. 2. Examples of localized one-, two-, and three-particle Frenkel states. For simplicity the molecules are numbered by one index n, instead of the unit-cell and sublattice index $\boldsymbol{n}\alpha$. (a) one-particle state $|n+1\ \overset{*}{1}\rangle$, (b) two-particle state $|n+1\ \overset{*}{1}\ (n\ 2)\rangle$, (c) three-particle state $|n+1\ \overset{*}{1}\ (n\ 2, n+2\ 1)\rangle$.

The expansion of the eigenfunctions in a series with consecutive terms representing the contributions from an increasing number of correlated particles, combined with the displaced-oscillator basis set, approaches the cumbersome region of intermediate vibronic interactions from the strong-coupling end. Nonetheless, as revealed by numerical tests, it converges reasonably well even a long way from the actual strong-coupling limit. For the system in hand, the three-particle configurations introduce merely small corrections of some quantitative relevance but with no qualitative impact.

Due to the translational symmetry, the Hamiltonian can be block-diagonalized using the Fourier transformation. The Frenkel states, Fourier transformed with respect to the exciton coordinate (the phonons positions being given relative to the exciton) are defined as

$$|\boldsymbol{k}, \alpha_1 \overset{*}{v}_1\rangle = N^{-1/2} \sum_{\boldsymbol{n}_1} e^{i\boldsymbol{k}\cdot\boldsymbol{n}_1} |\boldsymbol{n}_1 \alpha_1 \overset{*}{v}_1\rangle, \tag{14}$$

$$|\boldsymbol{k}, \alpha_1 \overset{*}{v}_1(\boldsymbol{m}\alpha_2 v_2)\rangle = N^{-1/2} \sum_{\boldsymbol{n}} e^{i\boldsymbol{k}\cdot\boldsymbol{n}} |\boldsymbol{n}\alpha_1 \overset{*}{v}_1(\boldsymbol{n}+\boldsymbol{m}\alpha_2 v_2)\rangle, \tag{15}$$

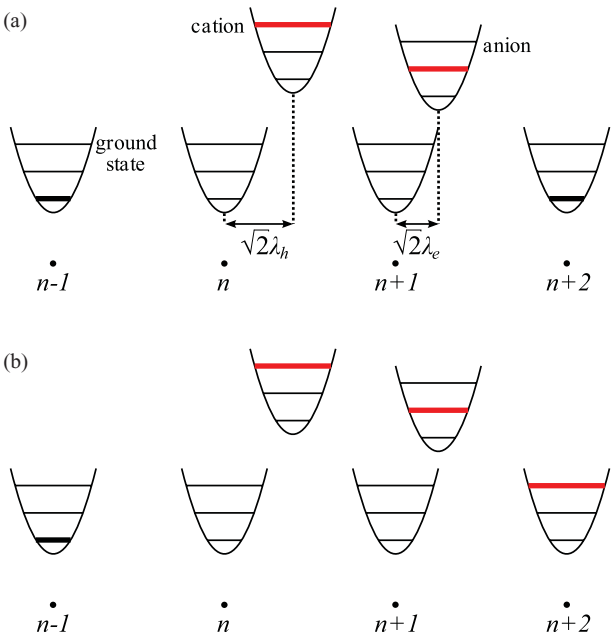

FIG. 3. Examples of localized two- and three-particle charge-transfer states. For simplicity the molecules are numbered by one index n, instead of the unit-cell and sublattice index $\boldsymbol{n}\alpha$. (a) two-particle state $|n\ \overset{+}{2}, n+1\ \overset{-}{1}\rangle$, (b) three-particle state $|n\ \overset{+}{2}, n+1\ \overset{-}{1}(n+2\ 2)\rangle$.

$$|\boldsymbol{k}, \alpha_1 \overset{*}{v}_1(\boldsymbol{m}_1\alpha_2 v_2, \boldsymbol{m}_2\alpha_3 v_3)\rangle = N^{-1/2} \sum_{\boldsymbol{n}} e^{i\boldsymbol{k}\cdot\boldsymbol{n}} |\boldsymbol{n}\alpha_1 \overset{*}{v}_1(\boldsymbol{n}+\boldsymbol{m}_1\alpha_2 v_2, \boldsymbol{n}+\boldsymbol{m}_2\alpha_3 v_3)\rangle, \tag{16}$$

while the CT states, Fourier-transformed with respect to the hole coordinate (with electron and phonon positions given relative to the hole), read

$$|\boldsymbol{k}, \alpha_1 \overset{+}{v}_1, \boldsymbol{m}\alpha_2 \overset{-}{v}_2\rangle = N^{-1/2} \sum_{\boldsymbol{n}} e^{i\boldsymbol{k}\cdot\boldsymbol{n}} |\boldsymbol{n}\alpha_1 \overset{+}{v}_1, \boldsymbol{n}+\boldsymbol{m}\alpha_2 \overset{-}{v}_2\rangle, \tag{17}$$

$$|\boldsymbol{k}, \alpha_1 \overset{+}{v}_1, \boldsymbol{m}_1\alpha_2 \overset{-}{v}_2(\boldsymbol{m}_2\alpha_3 v_3)\rangle = N^{-1/2} \sum_{\boldsymbol{n}} e^{i\boldsymbol{k}\cdot\boldsymbol{n}} |\boldsymbol{n}\alpha_1 \overset{+}{v}_1, \boldsymbol{n}+\boldsymbol{m}_1\alpha_2 \overset{-}{v}_2(\boldsymbol{n}+\boldsymbol{m}_2\alpha_3 v_3)\rangle, \tag{18}$$

In the above formulas, N denotes the number of unit cells and $\boldsymbol{k}$ is the total quasi-momentum of the exciton. In the Fourier-transformed basis set the Hamiltonian matrix is block-diagonal, with each block corresponding to a different value of quasi-momentum. The matrix elements that involve only the Frenkel states can be found in our previous papers,[14,15] while the remaining matrix elements are listed in Appendix A.

Only the block of the Hamiltonian that corresponds to total quasimomentum $\boldsymbol{k}$ equal zero is needed for the calculation of the optical spectra. However, for every value of $\boldsymbol{k}$ the three-particle basis set introduced above is infinite. In order to reduce the problem to numerically manageable size, we generalize the basis set truncation scheme introduced in Refs. 14 and 15 to encompass also the CT states. As previ-

ously, the total number of phonons ($\sum_i v_i$) is limited to η_{max}, the two-particle (three-particle) basis is truncated to finite size by including only those states where the distance between the molecules excited vibrationally and the molecule excited vibronically (in the case of Frenkel states) or any of the ionized molecules (in the case of CT states) does not exceed the cut-off radius r^{2F}_{max} (r^{3F}_{max}) for Frenkel states and r^{2CT}_{max} (r^{3CT}_{max}) for CT states.

The use of different cut-off radii for two- and three-particle basis set was discussed previously.[15] Different cut-off radii for the Frenkel and CT states are dictated by the vibronic coupling strength, different for these two types of excitations. To determine the optimum values of the cut-off parameters η_{max}, r^{2F}_{max}, r^{3F}_{max}, r^{2CT}_{max}, and r^{3CT}_{max} a series of calculations is performed, with gradual increase of the basis set size, until convergence is achieved.

III. SPECTRA

After the eigenstates of the Hamiltonian are found (both in the presence and in the absence of the external electric field), the absorption spectra can be readily calculated as

$$A(E, \boldsymbol{F}) = \frac{8\pi^3}{hcV} E \sum_i |\boldsymbol{\mu}_i(\boldsymbol{F}) \cdot \hat{\boldsymbol{e}}|^2 S_i(E), \tag{19}$$

where $\boldsymbol{\mu}_i(\boldsymbol{F})$ is the transition dipole moment to the ith eigenstate, $\hat{\boldsymbol{e}}$ is the polarization of the incident light, and $S_i(E)$ is a line-shape function centered at the energy E_i of the ith eigenstate, for most states assumed to be Gaussian,

$$S_i(E) = \frac{1}{\sqrt{2\pi}\sigma} \exp\left[-\frac{(E - E_i)^2}{2\sigma^2}\right]. \tag{20}$$

However, this shape function is not generally appropriate; evidently, it is not adequate for the strong absorption peak attributed to the upper Davydov component, which is diffuse and very broad. This fact is readily explicable, but not within the scheme introduced in Sec. II.

It should be borne in mind that the formalism presented there approaches the relevant region of intermediate vibronic coupling from the strong-coupling end. As indicated by the numerical instabilities detected at high energies,[15] the finite basis set described above is poorly suited to account for the behavior of the upper Davydov component, which is very intense and hence, weakly coupled to vibrations. The corresponding $\mathbf{k} = 0$ exciton, carrying only marginal lattice distortion,[15,17,19] is free to interact with the unbound exciton-phonon pairs deriving from the same upper Davydov band, but taken at other values of crystal momentum. There is a continuum of states to interact with: the potential interaction partners are all those pairs where the quasimomentum of the accompanying phonon exactly compensates the exciton quasimomentum, so that the net quasimomentum is zero. In spite of the small coupling constant, the effects of this interaction may be substantial, since, as follows from the dispersion relation, the $\mathbf{k} = 0$ exciton is immersed in the continuum, having exactly the same energy as some of the unbound pair states.

This problem has been treated recently[24,25] within the Fano model[26] to yield the following formula for the energy dependence of the absorption intensity, now spread over the continuum of one-phonon states,

$$I(E) = \frac{N\mu^2\gamma^2}{4C} \frac{1}{\left(E - E_\phi - \frac{\gamma^2}{4C} \ln\left(\frac{|E-\alpha|}{|E-\beta|}\right)\right)^2 + \frac{\pi^2\gamma^4}{16C^2}} \times \frac{1}{\frac{1}{\pi}\arctan\left(\frac{4C(\beta - E_\phi)}{\pi\gamma^2}\right) - \frac{1}{\pi}\arctan\left(\frac{4C(\alpha - E_\phi)}{\pi\gamma^2}\right)}, \tag{21}$$

where N is the number of molecules in the crystal, μ is the molecular transition dipole moment, $2C$ is the width of the exciton band, and E_ϕ is the energy of the discrete intensity-carrying state at $\mathbf{k} = 0$. Here, γ is an effective constant, governing the net spectral width and calculated from the Huang-Rhys factors of all vibronically active modes, as described in Ref. 24, while α and β delimit the energy continuum. In principle, it should cover all the energetic extent of the exciton band (shifted by one vibrational quantum with respect to the 0-0 line); in our implementation, it ends two quadrature points short of the actual band edges. This cut-off is used to circumvent the mild singularities that occur there because of the simplified density of states and is visually imperceptible. In order to smooth out the resultant discontinuities and at the same time account for the radiative width and inhomogeneous broadening, the actual absorption profile is calculated as the convolution of the envelope function of Eq. (21) with a Lorentzian shape function so narrow (0.004 eV) that the spectrum is insensitive to the change of its width. The resultant profile is ready to use here, while the details are to be found in Refs. 24 and 25.

Within the approach presented in Sec. II, the intensity of the upper Davydov component is distributed over a number of vibronic eigenstates. In order to use Eq. (19), we arbitrarily incorporate into one line all the transitions that appear in the range bracketed by the nearest predicted absorption minima, the line being located at their center of gravity (which should be identified with E_ϕ of Eq. (21)), and carrying their cumulative transition dipole moment, identified with μ of Eq. (21). To this effective spectral line, we attribute the shape defined by Eq. (20). In actual calculations, both E_ϕ and μ are further corrected to account for the systematic errors introduced by the Heitler-London approximation (HLA), underlying our present approach. As demonstrated some time ago,[27] for the specific value of the molecular transition dipole moment used throughout this paper, HLA overestimates the transition moment of the upper Davydov component by about 17%, and its energy by about 0.17 eV. To compensate the ensuing artifacts, we shift the effective E_ϕ to lower energies exactly by this amount and scale down the transition dipole moment accordingly.

The electroabsorption spectrum is calculated as the difference between the absorption spectrum in the presence of the external electric field and in its absence. Owing to the large width and diffuse profile of the continuum-broadened upper Davydov component, its contribution to the resultant

differential spectrum is very small and (based on numerical estimates) is consistently neglected.

IV. PARAMETRIZATION

The general theoretical framework presented above is applicable for a wide class of molecular crystals, including the actual structure of the sexithiophene low-temperature phase with four molecules in the unit cell. However, in order to reduce the enormous computational effort, we follow our previous papers on CT states[13] in taking explicitly into account only the two molecules that are contained in the same plane of 6T dense herringbone packing. In this way, we neglect the coupling mediated by small inter-plane CT integrals and ignore the two strictly forbidden gerade Davydov components. The values of the corresponding lattice sums indicate that in most cases the disregarded spectral features would not be discernible at the available experimental resolution. On this view, the approximation seems reasonable.

Wherever possible, our input is based on independent experimental data or calculations. However, the attainable accuracy of the computational methods used to evaluate some of the parameters is insufficient for the purposes of EA spectroscopy, which (as a differential technique) is very demanding in this regard. For these parameters, within the inherent error of our *a priori* estimates we tolerate some fine tuning, guided by the agreement of the simulated spectra with experiment. The same applies to the quantities estimated based merely on analogies. Most parameters barely deviate from those already reported in our previous papers, to which the reader is referred for details; here we just give a summary.

The vertical excitation energy of the Frenkel exciton (identified with the lowest B_u excitation of sexithiophene, corrected for gas-to-crystal shift) is set at 2.47 eV, i.e., slightly changed from the 2.45 eV of Refs. 14 and 15 to allow for CT-induced shifts, ignored there but explicitly included here. The corresponding transition dipole moment of 1.90 eÅ strictly follows our recent papers; so do the resonance integrals J and the ensuing lattice sums, evaluated within the submolecule version of the point-dipole approximation (each sexithiophene molecule being represented by a set of six dipoles). Independently derived exact formulas[28] are applied to generate the effective lattice sums for the model with two molecules per unit cell from those calculated for the complete crystal structure.

As previously, the quantum of the effective vibrational mode is set to 0.18 eV, with the dimensionless Franck-Condon parameter of 1.2. Following the estimate of Ref. 24, for the parameter that governs the broadening of the upper Davydov component on account of its interaction with the phonon continuum, we adopt the value of $\gamma = 1.7$ which encompasses the contributions from all totally symmetric modes of the molecule (calculated in Ref. 29), and is corrected for polariton effects based on the results of Ref. 27.

We are not aware of any reliable estimate of the sexithiophene molecular polarizability change upon electronic excitation. The values[12,30] resulting from EA experiments on crystals or films inevitably contain the nonlocal contribution (Ref. 31, vide infra), due to the off-diagonal mixing with CT states and automatically taken into account in our present model. The corresponding value including only the intramolecular contributions (relevant in the present context) could be obtained from EA experiments on 6T molecules in inert matrices. To our knowledge, no such experiments have been reported in the literature, and no calculated values are available either. On this view, our estimate is based on an analogy. For anthracene, the polarizability change upon excitation to the lowest singlet state is on the order of 20–30 Å^3. The 6T molecule is more than twice as large, but the pi-electron systems of its rings are somewhat less strongly coupled; overall, a polarizability change of about 25 Å^3 seems a reasonable guess, and this is the value we provisionally adopt. The effective electric field is calculated using the Lorentz factor of about 2 obtained as the average for the dielectric constants of 3.447 and 4.4, estimated in Ref. 32 from the experimental refractive index.[33]

This is consistent with the diagonal CT state energies used in the final reproduction of the spectra, which are bracketed between those resulting from microelectrostatic calculations[34] for the two above values of the dielectric constant; they are well within the anticipated error limits of the original estimates. In contrast to Ref. 13, our present values are corrected for the Stokes shift, explicitly included in the matrix elements of Appendix A. The diagonal dipole moments directly follow from lattice geometry; for the transition dipoles of the CT states we adopt the values of Ref. 34, based on analogies. Their order of magnitude is confirmed by crude semiempirical estimates, recently completed for the related 4T crystal.[35]

Independent evaluation of the displacement parameters λ_e, λ_h is by no means straightforward. Based on molecular orbital considerations,[1] the distortion parameter for positive or negative ionization is expected to be on the order of half the value appropriate for neutral molecule excitation, and definitely must not exceed the total value of the latter (which in our case is 0.85). Yet, it should be borne in mind that the 0.18 eV mode is an effective one. Its Franck-Condon parameter is merely a quantity reproducing the absorption envelope for a manifold of different vibrations, indirectly concocted from the shifts of the equilibrium positions in the ingredient modes between the ground and excited state of the molecule, with the weights based on the corresponding overlap integrals.

In principle, the same procedure could be applied to define the corresponding effective distortion parameter for the ionization process, using the shifts between the ground state of the ion and that of the neutral molecule. However, as indicated by the overlap integrals which appear in the matrix elements shown in the Appendix, in our calculations the shift of the equilibrium position between the ground state of the ion and the excited state of the molecule is equally important. In view of the role of anharmonicities and normal mode mixing, it is very unlikely that the weights of individual modes, needed to reproduce the corresponding effective quantity, would be the same as for unexcited molecule ionization. Hence, even if exact distortion parameters were known for the contributing modes, it still would not be obvious how to define the shift for the effective mode that would be

appropriate both for the integrals involving the ground and the excited state of the neutral molecule.

Density functional theory (DFT) calculations[36] confirm the involvement of several modes and reveal that in the linear approximation the shift in an individual mode is perceptibly different for ionization and for the reverse process, which is indicative of inter-mode mixing and/or anharmonic effects. Taking as a representative example the ingredient mode that is characterized by the largest displacement, the dimensionless shifts (for positive/negative ionization and for their reverse processes) range from 0.44 to 0.60. Their average of 0.52 is very close to the value of 0.54 yielding the optimum fit of the spectra shown in Sec. V, which seems plausible.

As previously, the CT integrals are evaluated from a tight-binding fit to band-structure calculations performed within the plane-wave version of the DFT approach. In order to reduce potential errors, in the new fit we now explicitly include some of the smaller, previously disregarded integrals. Although the latter do not appear in our model, their neglect in the fit might have affected the values of the integrals that do appear, and this procedure is meant to eliminate potential artifacts of this provenance. Indeed, some changes are noted. The final values are: $T^e_{12}(000) = 0.038$ eV, $T^h_{12}(000) = -0.017$ eV, $T^e_{11}(001) = 0.090$ eV, $T^h_{11}(001) = -0.010$ eV, $T^e_{11}(010) = 0.007$ eV, $T^h_{11}(010) = -0.002$ eV. The dissociation integrals are assumed equal to the corresponding electron or hole transfer integrals.

Based on convergence studies, all needed cut-off radii (r^{2F}_{max}, r^{3F}_{max}, r^{2CT}_{max}, r^{3CT}_{max}) have been set to 10 Å, with the phonon number cut-off $\eta_{max} = 6$. For the Gaussian shape functions of Eq. (20) the width of 0.025 eV is consistently used. It presumably accounts for inhomogeneous broadening and lattice relaxation and is roughly consistent with the estimate of this latter quantity in anthracene.[37] In reality, because of the growing density of states, the width is expected to increase with the energy of the pertinent transition, but we neglect this dependence in order to avoid the need to invoke an additional free parameter.

V. RESULTS

The neglected energy dependence of the spectral width has some influence on the rendering of the experimental *ac*-polarized spectrum, as shown in Fig. 4. By and large, the profile is very well reproduced, registering considerable improvement upon inclusion of the interaction with the exciton-phonon continuum (the uncorrected spectrum being shown in the main panel of the figure in reduced scale), but the features in the 2.5–3.0 eV range are still too sharp. The effect of underestimated width of individual high-energy states may be compounded by the consequences of the inherent limitation of the applied model, where only one Frenkel state per molecule is taken into account. According to theoretical calculations,[38] a forbidden intramolecular excited state is located just in the pertinent energy range and its coupling to the states that emerge from our model may well produce some extra broadening, at the same time shifting the calculated 2.8 eV absorption peak to slightly lower energies where it is experimentally observed.

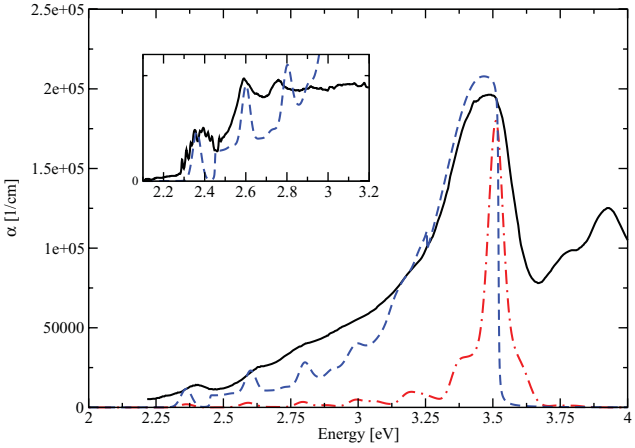

FIG. 4. Experimental (black solid line (Ref. 40)) and calculated (blue broken line) *ac*-polarized absorption spectra. The spectrum uncorrected for the interaction with exciton-phonon continuum (red dashed-dotted line) is shown in fivefold reduced scale.

As follows from eigenvector analysis, the *ac*-polarized eigenstates in the 2.5–3.0 eV range are of mixed origin; predominantly they are higher replicas of the Frenkel exciton, although some with considerable CT admixture. The nature of the absorption peak at about 3 eV is different: it is composed almost exclusively from CT configurations. The underestimated absorption intensity in that energy range is very likely due to the neglect of intensity borrowing from the short-axis polarized intramolecular excitation at about 3.7 eV,[39] not included in our model.

The above comments apply also to the *b*-polarized absorption spectrum, displayed in Fig. 5. While the predicted band energies and relative intensities are very reasonably reproduced, the total intensity of the spectrum and the widths of high-energy peaks are indubitably underestimated. An additional mechanism that may contribute to this behavior will be mentioned in Sec. VI.

A complete experimental electroabsorption spectrum is available only for *b* polarization; its theoretical reproduction is shown in Fig. 6. In view of its sensitivity to the shortcomings of the model, typical for differential spectra, theoreti-

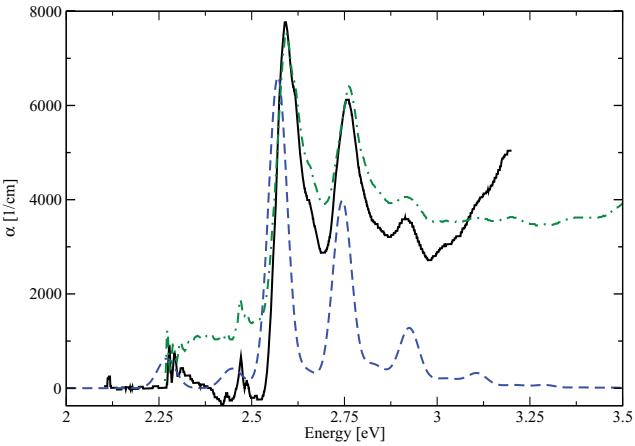

FIG. 5. Experimental (black solid (Ref. 40) and green dashed-dotted (Ref. 12) line) vs calculated (blue broken line) *b*-polarized absorption spectra.

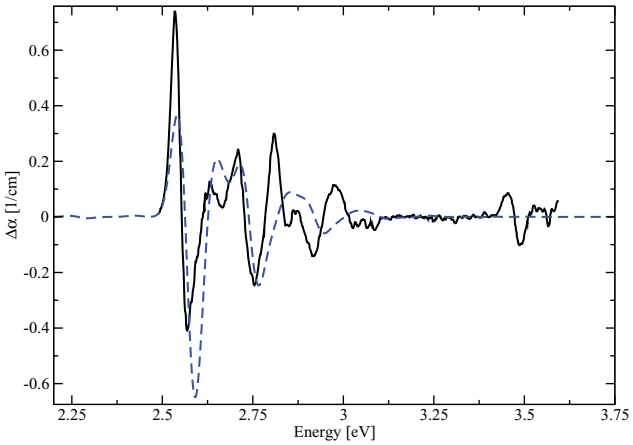

FIG. 6. Experimental (black solid line (Ref. 12)) and calculated (blue broken line) *b*-polarized electroabsorption spectra.

cal rendering of the experimental profile may be considered nearly perfect.

As separate figures, the original experimental paper on 6T electroabsorption[12] also features the high resolution EA signals in the immediate vicinity of the lower Davydov component (2.27 eV). The observed fine structure, due to low-frequency vibrations, is of course impossible to reproduce within our present model, where these modes are not included. However, as they are weakly coupled to the excitation,[19,41] for all of them the response to electric field should be the same and equal to the response of the $0-0$ line. This supposition is corroborated by the fact that the *b*-polarized EA signal perfectly coincides with the (judiciously scaled) first derivative of the corresponding absorption spectrum, as expected for nearly pure Frenkel exciton energetically distant from any other state. The scaling factor is governed by the value of the electric-field-induced shift, and this quantity is readily available from our results. For the applied field of 23 kV/cm the experimental shift is 0.3 μeV, well matched by the value of 0.31 μeV, predicted by our calculations for the vibrationally unexcited lower Davydov component. It is worth noting that about 85% of this value is due to the coupling with the CT manifold,[31] and only about 15% results from the change of the molecular polarizability upon electronic excitation.

Yet, for the lowest state in *ac*-polarization, located (according to the calculations) at 2.36 eV, the predicted shift is still larger, amounting to as much as 0.33 μeV for the experimentally applied weaker field of 19 kV/cm (the respective shift in *b* polarization being 0.21 μeV). In the adiabatic limit, this state would correspond to the phonon satellite in the effective 0.18 eV vibration. Its energy, higher than that of the $0-0$ line only by 0.1 eV, is a manifestation of the intermediate-coupling behavior of the pertinent mode. The increased field-induced shift has the same origin; the replica is closer to the CT manifold than the vibrational ground state, and for this reason is subject to stronger repulsion when the coupling via electric field is switched on.

Interestingly enough, experimental confirmation of this prediction is hidden in the existing experimental evidence, but seems to have been overlooked. Weiser *et al.*[12] show a very good fit of their low-energy EA signal in *ac* polarization by the (scaled) first derivative of the respective absorption spectrum, assuming the field-induced shift of 0.2 μeV (which agrees well with our calculated value of 0.21 μeV). However, upon closer scrutiny the fit turns out to be nearly perfect up to about 2.37 eV, and again from about 2.41 eV, while in the 2.37–2.41 eV range the amplitude of the scaled derivative is very small with respect to the observed EA signal (cf. Fig. 4 of Ref. 12). The authors generally blame the discrepancies on experimental noise, presumably large because of very low transmission. Admittedly, their spectrum exhibits a lot of noise, but beyond this specific range the latter is evidently the same for absorption and electroabsorption.

Our calculated results suggest the following interpretation. The fine structure below 2.37 eV is obviously due to vibronically induced satellites in weakly coupled low-frequency phonons, which mediate intensity borrowing from the upper Davydov component. With different phases on the two sublattices, these replicas derive from exactly the same intramolecular modes as those observed in *b* polarization (*vide supra*, Refs. 16,19, and 41), and are all built upon the same electronic origin (namely, the lower Davydov component). In view of their weak vibronic coupling, for all of them the response to electric field should again be the same as for the *b*-polarized $0-0$ line. In contrast, the replica in the 0.18 eV mode (owing to its relatively strong vibronic coupling) is affected by the decreased separation from the CT states, which results in its increased sensitivity to electric field, as revealed by our calculations. This makes the 0.18 eV mode stand out in the fit of Ref. 12, where the scaling factor of the absorption derivative is adjusted for the low-frequency vibrations; hence the experimental EA signal at about 2.37 eV seems to be inordinately strong.

In that energetic vicinity higher replicas in the low-frequency modes are also bound to contribute, with their normal (i.e., smaller) field-induced shift. Their explicit inclusion would be indispensable to reproduce the observed overall signal, which is beyond the scope of the present paper. It should be noted marginally that the higher precision standard needed to deal with low-frequency modes may in the future compel one to take into account the (so far disregarded) *gerade* Davydov components, of which the lower one is located less than 0.02 eV above the lower Davydov component of our model, as follows from a simple estimate based on the calculated lattice sums.[28] It is possible that the experimentally observed fine structure in the 2.37–2.41 eV range might contain (among other features) vibrational satellites in low-frequency phonons of the replica of that state in the 0.18 eV mode.

VI. DISCUSSION

The findings presented above contradict some commonly accepted posits of the conventional molecular exciton theory. First, it is commonly assumed that electronic characteristics of a molecule in such a crystal are only slightly affected by the crystalline environment. Second, this statement applies *a fortiori* to vibrationally excited states which (apart from marginal anharmonic corrections) are expected to exhibit the same properties as their parent molecular electronic state.

As shown above, the shift of the lowest 6T Frenkel exciton in electric field is much larger than it would be in an isolated molecule. The apparent polarizability change upon excitation to that state exceeds about seven times its molecular counterpart (which in the past led to claims of huge values of this latter quantity[12]). Moreover, for the $v = 1$ state in the main progression-forming mode, this value is increased by another factor of 1.6, i.e., is substantially larger than for the $0 - 0$ line. Obviously, this enormous sensitivity to electric field is not due to actual increase of molecular polarizability, but to a small admixture of CT configurations, endowed with large dipole moments. In the vibrationally excited state, this admixture is enhanced owing to the energetic proximity of the CT manifold.

Following conventional wisdom, the latter manifold is totally ignored in most interpretations of Frenkel exciton properties. This practice is justified for the ground state of the crystals (where, e.g., the polarizability differs only by about 10% from the free-molecule value[42]), but not for electronic excitations, where the coupling to CT states is strengthened owing to the reduced energy gap. The indirect influence of CT states on Frenkel excitons was first recognized in the late 1980s in a substantial CT-induced contribution to the Davydov splitting in polyacenes.[43] The original observation, based on a simplistic one-dimensional model, later turned out to be valid also in a more advanced framework,[20] and the effect has been independently rediscovered in recent sophisticated calculations of quantitative accuracy.[44] Meanwhile, CT contributions were indicated for pentacene as the cause of considerable anomalies in Frenkel exciton dispersion,[45] corroborating the earlier theoretical arguments. The effects of mixing between Frenkel and CT excitons, as well as their coupling to molecular vibrations, were investigated for perylene derivatives using one-dimensional model.[46]

A simplified model invoking the mixing with CT states was also used to explain the enhanced response of Frenkel states to electric field.[31] The specific estimates were done in the approximation of strong vibronic coupling, which probably precluded their quantitative accuracy. It should be noted marginally that the original version of the pertinent approach, disregarding the interaction between vibronic manifolds with different phonon number, was inherently incapable of reproducing the differences in the response of different vibrational levels of the Frenkel state, exposed by our present results.

The main objective of our present work was to consolidate the existing theory of charge transfer states with general description of vibronic effects. Owing to the short range of CT interactions, CT excitons, and their mixing with Frenkel excitons in crystals, such as 6T, was adequately described in terms of a two-dimensional model.[20] Unfortunately, in its original version the model could accommodate the vibronic interactions only in the limiting cases of weak or strong coupling. Besides, its actual implementation treated the exciton-resonance integrals in a simplistic way, modeling Davydov splitting merely by means of effective nearest-neighbor contributions, which distorted the balance between the short-range and long-range terms. On the other hand, the standard theory of vibronic effects in molecular crystals could not handle CT interactions, being correct only to zeroth order in intermolecular overlap integrals, whereas these interactions appear in the first order. Also the fact that a CT state engages two molecules made direct application of the standard Frenkel exciton theory impracticable. The present treatment is free from all these shortcomings.

In order to attain the quantitative agreement with experiment we have achieved here it was necessary to combine the two approaches mentioned above with several other stratagems, developed over the years. The recent study of the role of the exciton-phonon continuum was needed to explain the diffuse shape of the absorption spectrum,[24,25] explicit consideration of retardation effects providing an estimate of the polariton contribution to the ensuing broadening,[27] while the study of Frenkel excitons in classical formalism[47] gave an estimate of the corrections to the Heitler-London approximation,[27] indispensable to comply with the absolute energy scale and maintain the correct intensity balance. In addition, independent estimation of input parameters required some refinement of the methodologies rooted in quantum chemistry,[29,36] and improved fits of the previously calculated crystal band structures.[13]

By and large, the attained agreement with experiment seems very plausible, while the input data are well within the error limits set by the accuracy of the approaches used for parameter estimation, so that the overall picture is consistent and complete. The results correctly reproduce the *ac*-polarized absorption spectrum dominated by the vibronic structure of the Frenkel state, as well as the *b*-polarized absorption spectrum, mostly of CT origin. This was possible in neither of the two disjoint approaches integrated here. At the same time, good rendering of the interpretationally unforgiving *b*-polarized EA signal has also been achieved. These facts lend credence to the conclusions concerning the parentage of the *ac*-polarized absorption peaks at 2.6 eV and 2.78 eV: they are identified as vibronic satellites of predominantly Frenkel origin, although with some CT admixture. This indicates that their coincidence with the corresponding *b*-polarized bands (of purely CT origin) is accidental, which resolves the standing controversy. As an additional benefit, the EA amplitude is very well rendered without invoking unphysically large polarizability change between the ground and excited states of the molecule. We did not anticipate the extra bonus: the calculated field-induced shift of the *ac*-polarized vibronic replica at 2.36 eV, larger than that of the corresponding $0 - 0$ line, explains the discrepancies in the fit of the corresponding experimental EA signal by a scaled derivative of the absorption spectrum. The previous less complete approaches were inherently incapable of generating this result.

Admittedly, in some respects the simulated spectra still deviate from their experimental originals. Some peak energies are slightly off the mark and some intensity is missing in the 2.6–3.1 eV range of the *ac*-polarized absorption spectrum, which is probably due, at least partly, to the neglected coupling with higher Frenkel states (potentially possible to take into account in the future). This may also explain some intensity deficit in *b* polarization. In addition, some features of the experimental absorption spectra suggest that the crystal sample was either misaligned or twinned, which might explain the underestimated intensity and the presence of the contin-

uous background in the *b*-polarized spectrum in terms of a "leak" from *ac* polarization. In the future, the methodology presented here may be readily used to repeat the calculations for different crystal orientations and may be adapted to handle twinned crystals as well as disordered films. It is only to be hoped that the availability of this versatile interpretational tool will inspire new research in experimental EA spectroscopy.

ACKNOWLEDGMENTS

The authors express their gratitude to Dr. Marcin Andrzejak for access to his unpublished computational results concerning the Franck-Condon parameters and to Dr. Grzegorz Mazur for his calculations of the electronic overlap integrals. This work was financed from the Polish national resources allotted for research in the years 2009/2010 as statutory allocation (DS21) to the Faculty of Chemistry of the Jagiellonian University, and as research Grant No. N N204 316337 from the Ministry of Science and Higher Education. A.S. acknowledges the Netherlands Organization for Scientific Research for support through a VENI grant.

APPENDIX A: MATRIX ELEMENTS

The Hamiltonian matrix elements that involve two- and three-particle CT states assume the form

$$\begin{aligned}\langle \boldsymbol{k}, \alpha_1 \overset{+}{v}_1, \boldsymbol{n}\alpha_2 \bar{v}_2 | H | \boldsymbol{k}, \beta_1 \overset{+}{w}_1, \boldsymbol{m}\beta_2 \bar{w}_2 \rangle &= \delta_{\alpha_1,\beta_1}\delta_{\alpha_2,\beta_2}\delta_{v_1,w_1}\delta_{v_2,w_2}\delta_{\boldsymbol{n},\boldsymbol{m}}\left[E^{CT}_{\alpha_1\alpha_2\boldsymbol{n}} + \hbar\omega(v_1+v_2) - \hbar\omega\left(\lambda_h^2+\lambda_e^2\right)\right] \\ &+ \delta_{\alpha_2,\beta_2}\delta_{v_2,w_2}\left(1-\delta_{\alpha_1,\beta_1}\delta_{\boldsymbol{n},\boldsymbol{m}}\right)T^h\left(\boldsymbol{n}-\boldsymbol{m}+\boldsymbol{r}_{\beta_1}-\boldsymbol{r}_{\alpha_1}\right)e^{-i\boldsymbol{k}\cdot(\boldsymbol{n}-\boldsymbol{m})}(\overset{+}{v}_1|0)(0|\overset{+}{w}_1) \\ &+ \delta_{\alpha_1,\beta_1}\delta_{v_1,w_1}\left(1-\delta_{\alpha_2\beta_2}\delta_{\boldsymbol{n},\boldsymbol{m}}\right)T^e\left(\boldsymbol{m}-\boldsymbol{n}+\boldsymbol{r}_{\beta_2}-\boldsymbol{r}_{\alpha_2}\right)(\bar{v}_2|0)(0|\bar{w}_2), \end{aligned} \tag{A1}$$

$$\langle \boldsymbol{k}, \alpha_1 \overset{+}{v}_1, \boldsymbol{n}\alpha_2 \bar{v}_2 | H | \boldsymbol{k}, \beta \overset{*}{w} \rangle = \delta_{\alpha_2,\beta} D^h\left(\boldsymbol{n}+\boldsymbol{r}_{\beta}-\boldsymbol{r}_{\alpha_1}\right)e^{-i\boldsymbol{k}\cdot\boldsymbol{n}}(\overset{+}{v}_1|0)(\bar{v}_2|\overset{*}{w}) + \delta_{\alpha_1,\beta}D^e\left(-\boldsymbol{n}+\boldsymbol{r}_{\beta}-\boldsymbol{r}_{\alpha_2}\right)(\overset{+}{v}_1|\overset{*}{w})(\bar{v}_2|0), \tag{A2}$$

$$\begin{aligned}\langle \boldsymbol{k}, \alpha_1 \overset{+}{v}_1, \boldsymbol{n}\alpha_2 \bar{v}_2 | H | \boldsymbol{k}, \beta_1 \overset{*}{w}_1(\boldsymbol{m}\beta_2 w_2) \rangle &= \delta_{\alpha_1,\beta_2}\delta_{\alpha_2,\beta_1}\delta_{\boldsymbol{n},-\boldsymbol{m}}D^h\left(\boldsymbol{n}+\boldsymbol{r}_{\beta_1}-\boldsymbol{r}_{\alpha_1}\right)e^{-i\boldsymbol{k}\cdot\boldsymbol{n}}(\overset{+}{v}_1|w_2)(\bar{v}_2|\overset{*}{w}_1) \\ &+ \delta_{\alpha_1,\beta_1}\delta_{\alpha_2,\beta_2}\delta_{\boldsymbol{n},\boldsymbol{m}}D^e\left(-\boldsymbol{n}+\boldsymbol{r}_{\beta_1}-\boldsymbol{r}_{\alpha_2}\right)(\overset{+}{v}_1|\overset{*}{w}_1)(\bar{v}_2|w_2), \end{aligned} \tag{A3}$$

$$\begin{aligned}&\langle \boldsymbol{k}, \alpha_1 \overset{+}{v}_1, \boldsymbol{n}_1\alpha_2 \bar{v}_2(\boldsymbol{n}_2\alpha_3 v_3) | H | \boldsymbol{k}, \beta_1 \overset{+}{w}_1, \boldsymbol{m}_1\beta_2 \bar{w}_2, (\boldsymbol{m}_2\beta_3 w_3) \rangle \\ &= \delta_{\alpha_1,\beta_1}\delta_{\alpha_2,\beta_2}\delta_{\alpha_3,\beta_3}\delta_{v_1,w_1}\delta_{v_2,w_2}\delta_{v_3,w_3}\delta_{\boldsymbol{n}_1,\boldsymbol{m}_1}\delta_{\boldsymbol{n}_2,\boldsymbol{m}_2}\left[E^{CT}_{\alpha_1\alpha_2\boldsymbol{n}_1} + \hbar\omega(v_1+v_2+v_3) - \hbar\omega\left(\lambda_h^2+\lambda_e^2\right)\right] \\ &+ \delta_{\alpha_1,\beta_3}\delta_{\alpha_2,\beta_2}\delta_{\alpha_3,\beta_1}\delta_{v_2,w_2}\delta_{\boldsymbol{n}_1-\boldsymbol{n}_2,\boldsymbol{m}_1}\delta_{\boldsymbol{n}_2,-\boldsymbol{m}_2}T^h\left(\boldsymbol{n}_2+\boldsymbol{r}_{\beta_1}-\boldsymbol{r}_{\alpha_1}\right)e^{-i\boldsymbol{k}\cdot\boldsymbol{n}_2}(\overset{+}{v}_1|w_3)(v_3|\overset{+}{w}_1) \\ &+ \delta_{\alpha_1,\beta_1}\delta_{\alpha_2,\beta_3}\delta_{\alpha_3,\beta_2}\delta_{v_1,w_1}\delta_{\boldsymbol{n}_1,\boldsymbol{m}_2}\delta_{\boldsymbol{n}_2,\boldsymbol{m}_1}T^e\left(\boldsymbol{n}_2-\boldsymbol{n}_1+\boldsymbol{r}_{\beta_2}-\boldsymbol{r}_{\alpha_2}\right)(\bar{v}_2|w_3)(v_3|\bar{w}_2) \\ &+ \delta_{\alpha_2,\beta_2}\delta_{\alpha_3,\beta_3}\delta_{v_2,w_2}\delta_{v_3,w_3}\delta_{\boldsymbol{n}_1-\boldsymbol{n}_2,\boldsymbol{m}_1-\boldsymbol{m}_2}\left(1-\delta_{\alpha_1,\beta_1}\delta_{\boldsymbol{n}_1,\boldsymbol{m}_1}\right)T^h\left(\boldsymbol{n}_1-\boldsymbol{m}_1+\boldsymbol{r}_{\beta_1}-\boldsymbol{r}_{\alpha_1}\right)e^{-i\boldsymbol{k}\cdot(\boldsymbol{n}_1-\boldsymbol{m}_1)}(\overset{+}{v}_1|0)(0|\overset{+}{w}_1) \\ &+ \delta_{\alpha_1,\beta_1}\delta_{\alpha_3,\beta_3}\delta_{v_1,w_1}\delta_{v_3,w_3}\delta_{\boldsymbol{n}_2,\boldsymbol{m}_2}\left(1-\delta_{\alpha_2,\beta_2}\delta_{\boldsymbol{n}_1,\boldsymbol{m}_1}\right)T^e\left(\boldsymbol{m}_1-\boldsymbol{n}_1+\boldsymbol{r}_{\beta_2}-\boldsymbol{r}_{\alpha_2}\right)(\bar{v}_2|0)(0|\bar{w}_2), \end{aligned} \tag{A4}$$

$$\begin{aligned}&\langle \boldsymbol{k}, \alpha_1 \overset{+}{v}_1, \boldsymbol{n}_1\alpha_2 \bar{v}_2(\boldsymbol{n}_2\alpha_3 v_3) | H | \boldsymbol{k}, \beta_1 \overset{+}{w}_1, \boldsymbol{m}\beta_2 \bar{w}_2 \rangle \\ &= \delta_{\alpha_2,\beta_2}\delta_{\alpha_3,\beta_1}\delta_{v_2,w_2}\delta_{\boldsymbol{n}_1-\boldsymbol{n}_2,\boldsymbol{m}}T^h\left(\boldsymbol{n}_2+\boldsymbol{r}_{\beta_1}-\boldsymbol{r}_{\alpha_1}\right)e^{-i\boldsymbol{k}\cdot\boldsymbol{n}_2}(\overset{+}{v}_1|0)(v_3|\overset{+}{w}_1) \\ &+ \delta_{\alpha_1,\beta_1}\delta_{\alpha_3,\beta_2}\delta_{v_1,w_1}\delta_{\boldsymbol{n}_2,\boldsymbol{m}}T^e\left(\boldsymbol{n}_2-\boldsymbol{n}_1+\boldsymbol{r}_{\beta_2}-\boldsymbol{r}_{\alpha_2}\right)(\bar{v}_2|0)(v_3|\bar{w}_2), \end{aligned} \tag{A5}$$

$$\begin{aligned}&\langle \boldsymbol{k}, \alpha_1 \overset{+}{v}_1, \boldsymbol{n}_1\alpha_2 \bar{v}_2(\boldsymbol{n}_2\alpha_3 v_3) | H | \boldsymbol{k}, \beta_1 \overset{*}{w}_1(\boldsymbol{m}\beta_2 w_2) \rangle \\ &= \delta_{\alpha_2,\beta_1}\delta_{\alpha_3,\beta_2}\delta_{v_3,w_2}\delta_{\boldsymbol{n}_2-\boldsymbol{n}_1,\boldsymbol{m}}D^h\left(\boldsymbol{n}_1+\boldsymbol{r}_{\beta_1}-\boldsymbol{r}_{\alpha_1}\right)e^{-i\boldsymbol{k}\cdot\boldsymbol{n}_1}(\overset{+}{v}_1|0)(\bar{v}_2|\overset{*}{w}_1) \\ &+ \delta_{\alpha_1,\beta_1}\delta_{\alpha_3,\beta_2}\delta_{v_3,w_2}\delta_{\boldsymbol{n}_2,\boldsymbol{m}}D^e\left(-\boldsymbol{n}_1+\boldsymbol{r}_{\beta_1}-\boldsymbol{r}_{\alpha_2}\right)(\overset{+}{v}_1|\overset{*}{w}_1)(\bar{v}_2|0), \end{aligned} \tag{A6}$$

$$\begin{aligned}
&\langle \boldsymbol{k}, \alpha_1 \overset{+}{v}_1, \boldsymbol{n}_1\alpha_2 \overset{-}{v}_2(\boldsymbol{n}_2\alpha_3 v_3)|H|\boldsymbol{k}, \beta_1 \overset{*}{w}_1(\boldsymbol{m}_1\beta_2 w_2, \boldsymbol{m}_2\beta_3 w_3)\rangle \\
&= \delta_{\alpha_1,\beta_2}\delta_{\alpha_2,\beta_1}\delta_{\alpha_3,\beta_3}\delta_{v_3,w_3}\delta_{\boldsymbol{n}_1,-\boldsymbol{m}_1}\delta_{\boldsymbol{n}_2-\boldsymbol{n}_1,\boldsymbol{m}_2} D^h(\boldsymbol{n}_1 + \boldsymbol{r}_{\beta_1} - \boldsymbol{r}_{\alpha_1}) e^{-i\boldsymbol{k}\cdot\boldsymbol{n}_1} (\overset{+}{v}_1|w_2)(\overset{-}{v}_2|\overset{*}{w}_1) \\
&\quad + \delta_{\alpha_1,\beta_3}\delta_{\alpha_2,\beta_1}\delta_{\alpha_3,\beta_2}\delta_{v_3,w_2}\delta_{\boldsymbol{n}_1,-\boldsymbol{m}_2}\delta_{\boldsymbol{n}_2-\boldsymbol{n}_1,\boldsymbol{m}_1} D^h(\boldsymbol{n}_1 + \boldsymbol{r}_{\beta_1} - \boldsymbol{r}_{\alpha_1}) e^{-i\boldsymbol{k}\cdot\boldsymbol{n}_1} (\overset{+}{v}_1|w_3)(\overset{-}{v}_2|\overset{*}{w}_1) \\
&\quad + \delta_{\alpha_1,\beta_1}\delta_{\alpha_2,\beta_2}\delta_{\alpha_3,\beta_3}\delta_{v_3,w_3}\delta_{\boldsymbol{n}_1,\boldsymbol{m}_1}\delta_{\boldsymbol{n}_2,\boldsymbol{m}_2} D^e(-\boldsymbol{n}_1 + \boldsymbol{r}_{\beta_1} - \boldsymbol{r}_{\alpha_2}) (\overset{+}{v}_1|\overset{*}{w}_1)(\overset{-}{v}_2|w_2) \\
&\quad + \delta_{\alpha_1,\beta_1}\delta_{\alpha_2,\beta_3}\delta_{\alpha_3,\beta_2}\delta_{v_3,w_2}\delta_{\boldsymbol{n}_1,\boldsymbol{m}_2}\delta_{\boldsymbol{n}_2,\boldsymbol{m}_1} D^e(-\boldsymbol{n}_1 + \boldsymbol{r}_{\beta_1} - \boldsymbol{r}_{\alpha_2}) (\overset{+}{v}_1|\overset{*}{w}_1)(\overset{-}{v}_2|w_3),
\end{aligned} \tag{A7}$$

where $(\overset{*}{v}|w)$, $(\overset{+}{v}|w)$, $(\overset{-}{v}|w)$ denote the overlap integrals between the vibrational wavefunction with v phonons in the displaced potential of the molecular excited, cationic, or anionic state and the vibrational wavefunction with w phonons in the electronic ground state of the neutral molecule, while $(\overset{+}{v}|\overset{*}{w})$, $(\overset{-}{v}|\overset{*}{w})$ denote the overlap integral between the vibrational wavefunctions in two diplaced potentials: with v phonons for the ionized state and w phonons for the electronic excited state.

APPENDIX B: NOTATION

In order to facilitate the comparison of the model presented here with older work on electroabsorption spectra of oligoacene and oligothiophene crystals,[13,20] Table I shows the correspondence between the notation used for the excited state creation operators in the older papers and in the current one.

TABLE I. Translation between the notation for creation operators from older papers (Refs. 13 and 20) and the current paper. Since the dense-packing crystallographic planes are bc plane for sexithiophene and ab plane for oligoacenes, we denote $\boldsymbol{n} = (l, m, 0)$ for sexithiophene and $\boldsymbol{n} = (0, l, m)$ for oligoacenes; $\boldsymbol{a}$, $\boldsymbol{b}$, and $\boldsymbol{c}$ denote the unit vectors along the respective crystallographic axes, σ denotes the sublattice (1 or 2).

	This paper	
Old papers	Sexithiophene	Oligoacenes
$B^\dagger_{\sigma lm}$	$A^\dagger_{\boldsymbol{n}\,\sigma}$	$A^\dagger_{\boldsymbol{n}\,\sigma}$
$P^\dagger_{1lm}$	$X^\dagger_{\boldsymbol{n}\,1,\boldsymbol{n}\,2}$	$X^\dagger_{\boldsymbol{n}\,1,\boldsymbol{n}\,2}$
$P^\dagger_{2lm}$	$X^\dagger_{\boldsymbol{n}\,2,\boldsymbol{n}\,1}$	$X^\dagger_{\boldsymbol{n}\,2,\boldsymbol{n}\,1}$
$R^\dagger_{1lm}$	$X^\dagger_{\boldsymbol{n}\,1,\boldsymbol{n}-\boldsymbol{b}\,2}$	$X^\dagger_{\boldsymbol{n}-\boldsymbol{a}\,1,\boldsymbol{n}\,2}$
$R^\dagger_{2lm}$	$X^\dagger_{\boldsymbol{n}\,2,\boldsymbol{n}+\boldsymbol{b}\,1}$	$X^\dagger_{\boldsymbol{n}+\boldsymbol{a}\,2,\boldsymbol{n}\,1}$
$S^\dagger_{1lm}$	$X^\dagger_{\boldsymbol{n}\,1,\boldsymbol{n}-\boldsymbol{b}-\boldsymbol{c}\,2}$	$X^\dagger_{\boldsymbol{n}-\boldsymbol{a}-\boldsymbol{b}\,1,\boldsymbol{n}\,2}$
$S^\dagger_{2lm}$	$X^\dagger_{\boldsymbol{n}\,2,\boldsymbol{n}+\boldsymbol{b}+\boldsymbol{c}\,1}$	$X^\dagger_{\boldsymbol{n}+\boldsymbol{a}+\boldsymbol{b}\,2,\boldsymbol{n}\,1}$
$T^\dagger_{1lm}$	$X^\dagger_{\boldsymbol{n}\,1,\boldsymbol{n}-\boldsymbol{c}\,2}$	$X^\dagger_{\boldsymbol{n}-\boldsymbol{b}\,1,\boldsymbol{n}\,2}$
$T^\dagger_{2lm}$	$X^\dagger_{\boldsymbol{n}\,2,\boldsymbol{n}+\boldsymbol{c}\,1}$	$X^\dagger_{\boldsymbol{n}+\boldsymbol{b}\,2,\boldsymbol{n}\,1}$
$L^\dagger_{\sigma lm\pm1}$	...	$X^\dagger_{\boldsymbol{n}\,\sigma,\boldsymbol{n}\pm\boldsymbol{b}\,\sigma}$
$L^{c\dagger}_{\sigma lm\pm1}$	$X^\dagger_{\boldsymbol{n}\,\sigma,\boldsymbol{n}\pm\boldsymbol{c}\,\sigma}$	...
$L^{b\dagger}_{\sigma lm\pm1}$	$X^\dagger_{\boldsymbol{n}\,\sigma,\boldsymbol{n}\pm\boldsymbol{b}\,\sigma}$	...

[1] P. J. Bounds, W. Siebrand, and P. Petelenz, Chem. Phys.**63**, 303 (1981).
[2] P. Petelenz, V. H. Smith, Jr., J. Klein, P. Martin, and R. Voltz, Chem. Phys. **112**, 457 (1987).
[3] R. E. Merrifield, J. Chem. Phys. **34**, 1835 (1961).
[4] S. Tavazzi, M. Laicini, L. Raimondo, P. Spearman, A. Borghesi, A. Papagni, and S. Trabattoni, Appl. Surf. Sci. **253**, 296 (2006).
[5] L. Sebastian, G. Weiser, and H. Bässler, Chem. Phys. **61**, 125 (1981).
[6] L. Sebastian, G. Weiser, G. Peter, and H. Bässler, Chem. Phys. **75**, 103 (1983).
[7] P. Petelenz, in *Proceedings of the International School of Physics "Enrico Fermi," Course CXLIX*, edited by V. M. Agranovich and G. C. La Rocca (IOS Press, Amsterdam, 2002), pp 1–25.
[8] *Handbook of Conducting Polymers*, edited by T. A. Scotheim (Marcel Dekker, New York, 2007), Vols. 1 and 2.
[9] *Handbook of oligo- and poly-thiophenes*, edited by D. Fichou (Wiley-VCH, Weinheim, 1999).
[10] G. Horowitz, D. Fichou, X. Peng, Z. Xu, and F. Garnier, Solid State Commun. **72**, 381 (1989).
[11] A. Dodabalapur, L. Torsi, and H. E. Katz, Science **268**, 270 (1995).
[12] S. Möller, G. Weiser, and F. Garnier, Phys. Rev. B **61**, 15749 (2000).
[13] M. Andrzejak, P. Petelenz, M. Slawik, and R. W. Munn, J. Chem. Phys. **117**, 1328 (2002).
[14] A. Stradomska and P. Petelenz, J. Chem. Phys. **130**, 094705 (2009).
[15] A. Stradomska and P. Petelenz, J. Chem. Phys. **131**, 044507 (2009).
[16] P. Petelenz and M. Andrzejak, J. Chem. Phys. **113**, 11306 (2000).
[17] F. C. Spano, J. Chem. Phys. **118**, 981 (2002).
[18] F. C. Spano, J. Chem. Phys. **120**, 7643 (2004).
[19] Z. Zhao and F. C. Spano, J. Chem. Phys. **122**, 114701 (2005).
[20] P. Petelenz, M. Slawik, K. Yokoi, and M. Z. Zgierski, J. Chem. Phys. **105**, 4427 (1996).
[21] R. W. Munn, Chem. Phys. **236**, 151 (1998).
[22] I. G. Lang and Y. A. Firsov, Zh. Eksp. Teor. Fiz. **43**, 1843 (1962).
[23] M. R. Philpott, J. Chem. Phys. **55**, 2039 (1971).
[24] W. Kulig and P. Petelenz, Phys. Rev. B **79**, 094305 (2009).
[25] P. Petelenz and W. Kulig, Chem. Phys. **343**, 100 (2008).
[26] U. Fano, Phys. Rev. **124**, 1866 (1961).
[27] A. Stradomska and P. Petelenz, Acta Physica Polonica A **112**, S161 (2007).
[28] A. Stradomska, Ph.D. dissertation (Jagiellonian University, 2008).
[29] M. Andrzejak and M. Pawlikowski, J. Phys. Chem. A **112**, 13737 (2008).
[30] L. M. Blinov, S. P. Palto, G. Ruani, C. Taliani, S. A. A. Tevosov, G. Yudin, and R. Zamboni, Chem. Phys. Lett. **232**, 401 (1995).
[31] P. Petelenz, Chem. Phys. Lett. **215**, 607 (1993).
[32] M. Andrzejak and P. Petelenz, Synth. Met. **109**, 97 (2000).
[33] G. Horowitz, S. Romdhane, H. Bouchriha, P. Delannoy, J.-L. Monge, F. Kouki, and P. Valat, Synth. Met. **90**, 187 (1997).
[34] M. Andrzejak and P. Petelenz, Mol. Cryst. Liq. Cryst. **355**, 65 (2001).
[35] G. Mazur, M. Slawik, and P. Petelenz (unpublished).
[36] M. Andrzejak, W. Kulig, and P. Kubisiak (unpublished).
[37] I. V. Brovchenko, Chem. Phys. Lett. **278**, 355 (1997).
[38] D. Beljonne, Z. Shuai, and J.-L. Bredas, J. Chem. Phys. **98**, 8819 (1993).
[39] D. Oelkrug, H.-J. Egelhaaf, and J. Haiber, Thin Solid Films **284**, 267 (1996).
[40] M. A. Loi, C. Martin, H. R. Chandrasekhar, M. Chandrasekhar, W. Graupner, F. Garnier, A. Mura, and G. Bongiovanni, Phys. Rev. B **66**, 113102 (2002).

[41]Z. Zhao and F. C. Spano, J. Phys. Chem. C **111**, 6113 (2007).
[42]R. W. Munn and P. Petelenz, Chem. Phys. Lett. **392**, 7 (2004).
[43]B. Petelenz, P. Petelenz, H. F. Shurvell, and V. H. Smith, Jr., Chem. Phys. **119**, 25 (1988).
[44]H. Yamagata, J. Norton, E. Hontz, Y. Olivier, D. Beljonne, J. L. Brédas, R. J. Silbey, and F. C. Spano, J. Chem. Phys. **134**, 204703 (2011).
[45]R. Schuster, M. Knupfer, and H. Berger, Phys. Rev. Lett. **98**, 037402 (2007).
[46]M. Hoffmann and Z. G. Soos, Phys. Rev. B **66**, 024305 (2002).
[47]A. Stradomska and P. Petelenz, Org. Electron. **7**, 551 (2006).
[48] In fact, the EA spectra were also recorded for the single crystals of polydiacetylene derivatives and of the Anthracene – Polymellitic Dianhydride (Anthr-PMDA) donor-acceptor complex. The former being a polymer and the latter being a two-component system, their physics is quite different from the case under consideration here, which leaves the EA spectrum of 6T as the only single-crystal spectrum pertinent in the present context.